nature nanotechnology

SUPPLEMENTARY INFORMATION

DOI: 10.1038/NNANO.2015.198

Hierarchically arranged helical fibre actuators driven by solvents and vapours

*Peining Chen, Yifan Xu, Sisi He, Xuemei Sun, Shaowu Pan, Jue Deng, Daoyong Chen, Huisheng Peng**

This PDF file includes:

Supplementary Notes

1. Twisted turns inserted into the fibre

The total numbers of twisting turns inserted into a primary fibre, single-ply helical fibre (SHF) with a coiled structure twisted from stacked MWCNT sheets, and HHF were calculated according to the spinning speed and consuming time during the preparation process. For example, a primary fibre with a helical angle of 32 °is spun at a rotary speed of 2,000 rpm and further collected by a rotating drum with a linear speed of 15 cm/min, so the number of twisted turns (T) into the primary fibre is T = 2,000/15 ≈ 133.3 turns per centimetre. The diameter and density of the primary fibre are 15 μm and 0.54 g/cm^3, respectively. Therefore, the number of turns inserted into the fibre is calculated as 1.4 × 10^8 turns/g. It takes about 9 minute to twist 20 layers of stacked MWCNT sheets (with the same length of 20 cm) into an SHF with a spinning speed of 200 rpm. The mass of the SHF is 380 μg, so the number of twisted turns into the SHF is calculated as 4.7 × 10^6 turns/g. For an HHF twisted from 20 primary fibres sharing a primary helical angle of 32 °, the twisted turns inserted into the fibre are divided into two parts, i.e., pre-existing twisting turns in the primary fibres and additional twisting turns inserted into the HHF during the twisting of primary fibres. The mass of the 20 primary fibres with a length of 20 cm is 380 μg, so the pre-existing twisted turns stored in the primary fibres can be calculated as 5.32 × 10^4 turns. It takes about 7.5 minute to twist above primary fibres into an HHF with a rotating speed of 200 rpm. The number of additional twisting turns is calculated as 1,500. Therefore, the total number of twisted turns stored in the HHF can be calculated as 5.47 × 10^4, i.e., 1.44 × 10^8 turns/g. The number of the twisted turns inserted in the HHF is over 30 times of the SHF twisted from stacked MWCNT sheets.

2. Mechanical properties

The strain of HHF was much higher than the primary fibre. For instance, an HHF twisted from 20 left-handed primary fibres with a helical angle of 32 ° had produced a strain of 240%, more than 60 times of the building primary fibre (Supplementary Fig. 22). The strain at the breaking point was increased with the increasing helical angle of the building primary fibre, while the strength (the stress at breaking) was first increased and then decreased with the increasing helical angle with a peak value of 212 MPa appearing at 32 ° (Supplementary Fig. 23). The fracture cross section of the HHF twisted from non-helical primary fibres was found to be more uniform compared with the HHF prepared from helical primary fibres (Supplementary Fig. 24),

which was consistent with the lower mechanical strength of the former. The breaking energy of the HHF was also dependent on the helical angle of primary fibre, and a peak value of 74 J/g had been observed at 32 °(Supplementary Fig. 25).

3. Actuations affected by primary helical angle

For a primary fibre, the generated contractive stresses were firstly increased and then decreased with increasing helical angles upon coming into contact with a droplet of ethanol (Supplementary Fig. 26), and a peak value of 2.8 MPa occurred at a helical angle of 32 °, which is consistent with the effect of microfibril helical angle on the contractive behaviour of cylindrical cells in plants[S1] (Supplementary Fig. 27). The primary fibres were then used to construct the HHF. As expected, a similar dependence of primary helical angle on the maximum contractive stress generated by HHF had been demonstrated, and a peak value of ~1.5 MPa was observed at the primary helical angle of 32 ° (Supplementary Fig. 6). The contractive stress generated by the HHF was smaller than that of a primary fibre. This difference may be attributed to the decreased tensile moduli of the HHFs after the formation of coils inside (Supplementary Fig. 22).

4. Actuations affected by diameters and lengths

The HHFs twisted from 10, 20 and 40 primary fibres displayed increasing diameters of 40 μm, 65 μm and 82 μm, respectively (Supplementary Fig. 28). Upon coming into contract with a droplet of ethanol and under the same other condition, the generated contractive stresses remained almost unchanged with the increasing fibre diameters as the generated contractive force and cross-sectional area are both increased. For the longer HHF, a higher capacity was provided for the solvent infiltration, so more surface free energy was released and transferred to actuation energy. Therefore, a higher contractive stress was generated from a longer fibre.

5. Torsional torque and power output

The moment of inertia of a thin cubical copper paddle is calculated as 2×10^{-10} kg·m^2 according to Supplementary Equation (1).

$$J = \frac{1}{12} \mathrm{m} L^2 \qquad (1)$$

where m and L correspond to the mass (79 mg) and length (5.5 mm) of the cooper paddle, respectively. The average acceleration (α) of the paddle in the initial 0.11 s (Supplementary Fig.

9) was calculated as 378 rad/s^2 (21,662 °/s^2). The mass of the used HHF was ~120 μg. Therefore, the produced initial torsional torque was calculated by $\tau = J\alpha$ = 7.56 × 10^{-8} N m, i.e., 630 mN m/Kg.

The rotatory speed of the stationary copper paddle was accelerated to a maximum, i.e., ω = 133 rad/s (7,634 °/s) in a short period of 0.495s (t), so the generated peak power output of the rotatory copper paddle is calculated to be 29.7 W/kg from Supplementary Equation (2).

$$P = \frac{W}{t} = \frac{J\omega^2}{2t} \qquad (2)$$

The rotational work output during the whole rotatory process could be expressed by Supplementary Equation (3),

$$W_R = \frac{1}{2} J \int \omega^2 dt \qquad (3)$$

where the integration of ω^2 over t can be calculated from the blue area in Supplementary Fig. 29, i.e., 16,392 (rad/s)^2. The mass and density of the actuating HHF were ~120 μg and 540 kg/m^3, respectively. Therefore, W_R is calculated as 13.7 J/kg or 7.4 kJ/m^3. Meanwhile, a maximum contraction of ~10% was observed during the rotation, so the contractive work output for the HHF could be calculated as 12.9 J/kg or 7 kJ/m^3 by Supplementary Equation (4),

$$W_C = mgh \qquad (4)$$

where m, g and h correspond to the mass of copper paddle, gravitational acceleration and contractive length of actuating fibre, respectively. Therefore, the total work output in response to ethanol is 26.6 J/kg or 14.4 kJ/m^3.

6. Actuation mechanism

For a single helix under volume expansion, the lengthwise contraction is generated when its helical angle is less than a critical value of ~54 °[S2]. There are two levels of helical units, i.e., MWCNTs and primary fibres in the HHF, and the helical angles at the two levels are both less than the critical value. Therefore, the helices expand in the radial direction and contract along the lengthwise direction as the volume of the fibre is increased (Supplementary Fig. 30). Simultaneously, a rotary actuation in the untwisting direction will be generated, similar to the hydraulically or pneumatically driven torsional actuation in unbalanced McKibben muscles [S3].

The infiltration of the solvent into the fibre depends on the surface wetting property of MWCNTs. It has been demonstrated that the contact angles of various organic solvents against MWCNTs are far below 90 °. The fibres thus can be rapidly wetted according to Young's

Equation:

$$\gamma_{vs} = \gamma_{ls} + \gamma_{vl}\cos\theta \qquad (5)$$

where γ_{vs}, γ_{ls} and γ_{vl} correspond to the surface free energies (surface tensions) of the vapour-solid, liquid-solid and vapour-liquid interfaces, respectively, and θ is the contact angle between the liquid and solid surface. In the case of actuation in response to a vapour, the volume expansion may be caused by the capillary condensation generated in the nano-scale gaps within the HHF. The diffusion of ethanol in the helical gaps is driven by capillary force that can be expressed as $F_d = \gamma_{vs} - \gamma_{ls}$ [S4]. As expected, in the event that an HHF comes into contact with an ethanol/aqueous mixture, the driving force of the ethanol/water mixture will be decreased with the increasing water volume fraction because of the higher liquid-solid interface tension of water (γ_{ls} = 90.6 mN·m^{-1}). Consequently, the amount of solvent infiltrated into the HHF is reduced and the generated contractive and rotary actuations are weakened, which agrees with the Supplementary Fig. 31. Furthermore, no contractive or rotary actuations were observed below 20 vol% ethanol because the driving force was too weak to allow solvent infiltration into the gaps.

The energy for the contractive and rotary actuations may originate from the surface free energy that is released during the wetting process, in which air-solid interfaces are rapidly replaced by liquid-solid interfaces. The kinetic energy thus generated is expressed by Supplementary Equation (6):

$$W_k = -\Delta G = \gamma_{vs} + \gamma_{vl} - \gamma_{ls} \qquad (6)$$

where ΔG represents the change in the Gibbs free energy during the wetting process. Combining Supplementary Equation (6) and Young's Equation, we may obtain:

$$W_k = \gamma_{vl}(\cos\theta + 1) \qquad (7)$$

MWCNTs exhibit a high specific surface area at the order of 10^2 m^2/g, and the surface free energy of the vapour-liquid interface for ethanol is ~22 mJ/m^2 [S5]. If the contact angle between the ethanol and fibre is 23.9 ° [S4], the amount of released surface free energy can be estimated to be 3 kJ/kg. The total work output in response to ethanol is 26.6 J/kg, so the energy-conversion efficiency of the HHF was calculated to be ~1%.

The surface free energy has been also transferred to other forms of energy such as the elastic energy. To calculate the elastic energy [S6], two ends of an HHF (with a length of 2 cm) were fixed on the clamp of the HY0350 Table-top Universal Testing Instrument with an applied stress

of 1.5 MPa. Upon coming into contract with a droplet of ethanol, the fibre generated a contractive stress of 1.2 MPa. Under the ethanol infiltration, the contractive stress and virtual strain were traced by moving down the upper clamp with a rate of 1 mm/min. As shown in Supplementary Fig. 32, the contractive stress was completely released as the virtual strain reached ~12%. According to the virtual work principle, the elastic energy (W_E) stored in the HHF can be calculated as 144 KJ/m^3 (267 J/kg) by Supplementary Equation (8), accounting for 9% of the released surface free energy.

$$W_E = \sigma\varepsilon \qquad (8)$$

where σ and ε correspond to the contractive stress and virtual strain, respectively. Besides elastic energy and actuation energy, the surface free energy might be transferred to gravitational potential energy and kinetic energy for the solvent diffusion in the gap.

7. The use as a generator

By virtue of the rapid rotations exhibited by the HHFs in response to solvents, they can be used to fabricate alternating-current generators. As shown in Supplementary Fig. 21, a homemade copper coil (100 turns) with a diameter of 1.3 cm was connected at one end of an HHF (with a length of 4 cm) prepared from 50 primary fibres. The copper coil was then placed in a magnetic field produced by a bar magnet. Here the actuating HHF also served as a conductive wire because of its high electrical conductivity. When the HHF was sprayed with ethanol, alternating currents had been generated by the reversible forward and reverse rotations of the fibre (Supplementary Fig. 21b). The number of forward revolutions was approximately equal to the number of reverse revolutions (Supplementary Fig. 21c). The low number of revolutions (9 turns) might be attributed to the restriction imposed by the fact that the external conductive wire was connected to the copper coil. It was found that the rapid wetting process (forward rotation) contributed more to the generated current than the evaporation process (reverse rotation), and a peak current output of 0.11 mA was observed during a forward rotation.

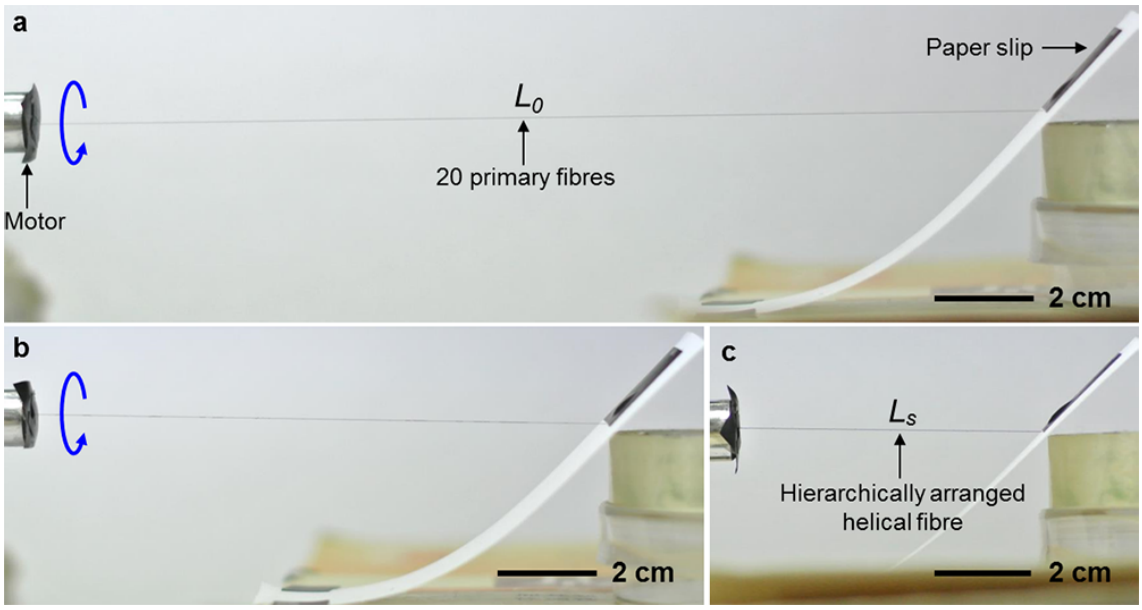

Supplementary Fig. 1. Photographs of the experimental setup to prepare an HHF. **a**, 20-ply primary fibres bundled together with one end stabilized at a rotating motor shaft and the other at a movable paper slip. The primary fibres shared a length of 20 cm. **b**, Rotation of the motor to produce an HHF. During the twisting process, the fibres were kept horizontal to be stretched by moving the paper slip toward the motor. **c**, An HHF with a length of ~5 cm from **a**. Here L_0 and L_s correspond to the lengths of the fibre before and after twisting, respectively.

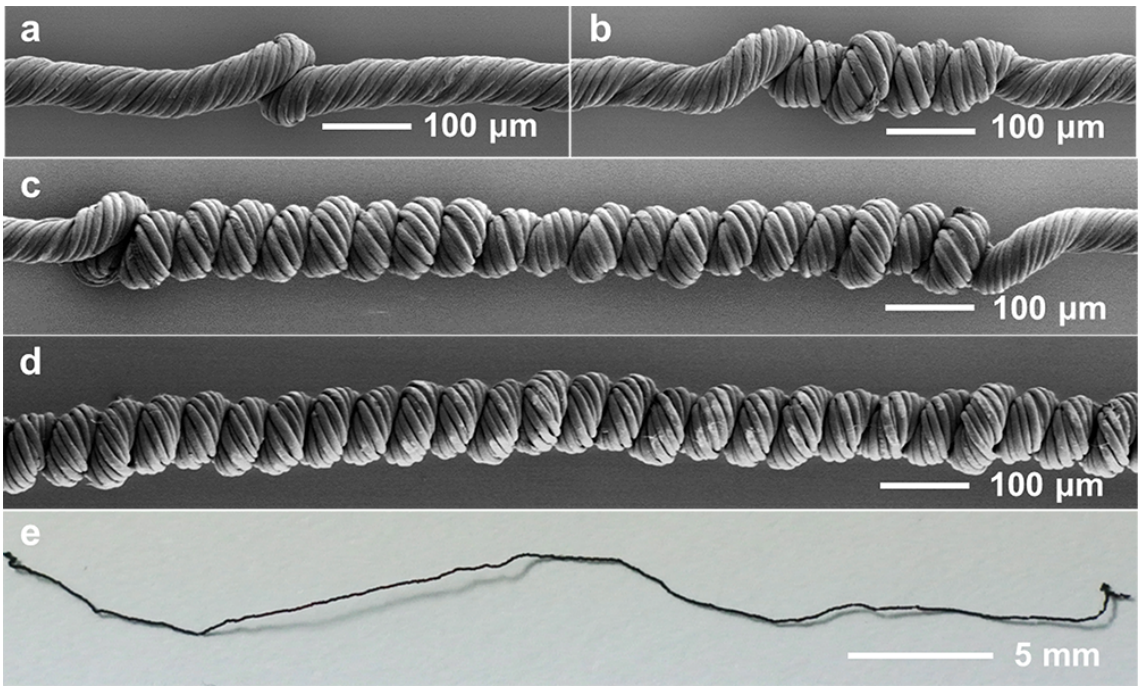

Supplementary Fig. 2. Morphology evolution to form an HHF during a twisting process under scanning electron microscopy (SEM). **a**, The first coil being formed when the inserted number of turns exceeded a certain critical value. The primary fibres were helically organized. **b** and **c**, The coils being formed sequentially along the axial direction. The coils were compactly arranged. **d**, A continuous, free-standing HHF. The coils exhibited an average diameter of 105 μm. **e**, Photograph of a continuous HHF at a relaxing state. The resulting fibre was structurally stable and no obvious partial entwisting or untwisting has been observed.

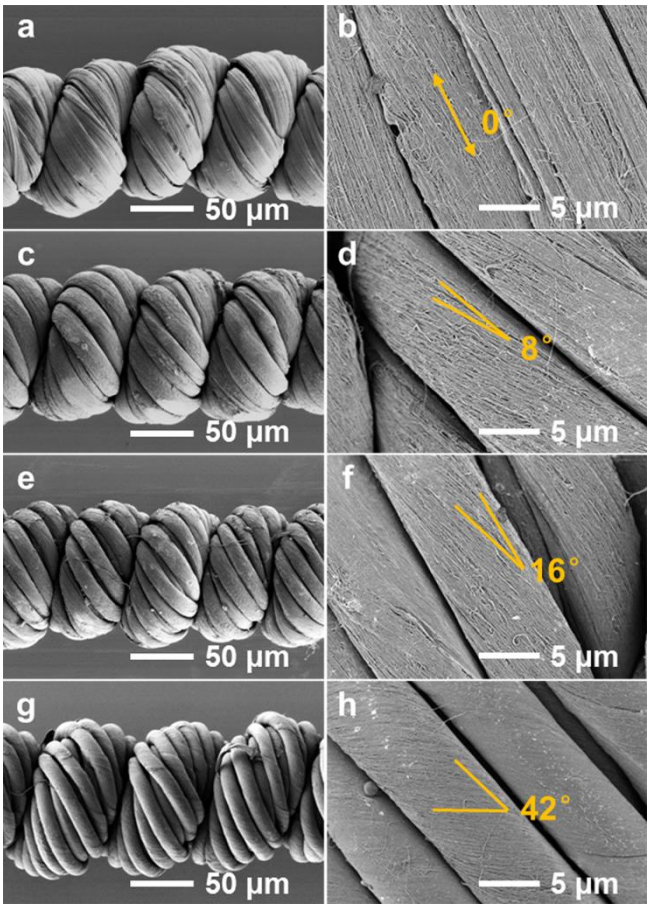

Supplementary Fig. 3. SEM images of HHFs prepared from primary fibres with helical angles of 0 ° (**a**, **b**), 8 ° (**c**, **d**), 16 ° (**e**, **f**) and 42 ° (**g**, **h**). The HHFs were composed of the same number (20) of primary fibres.

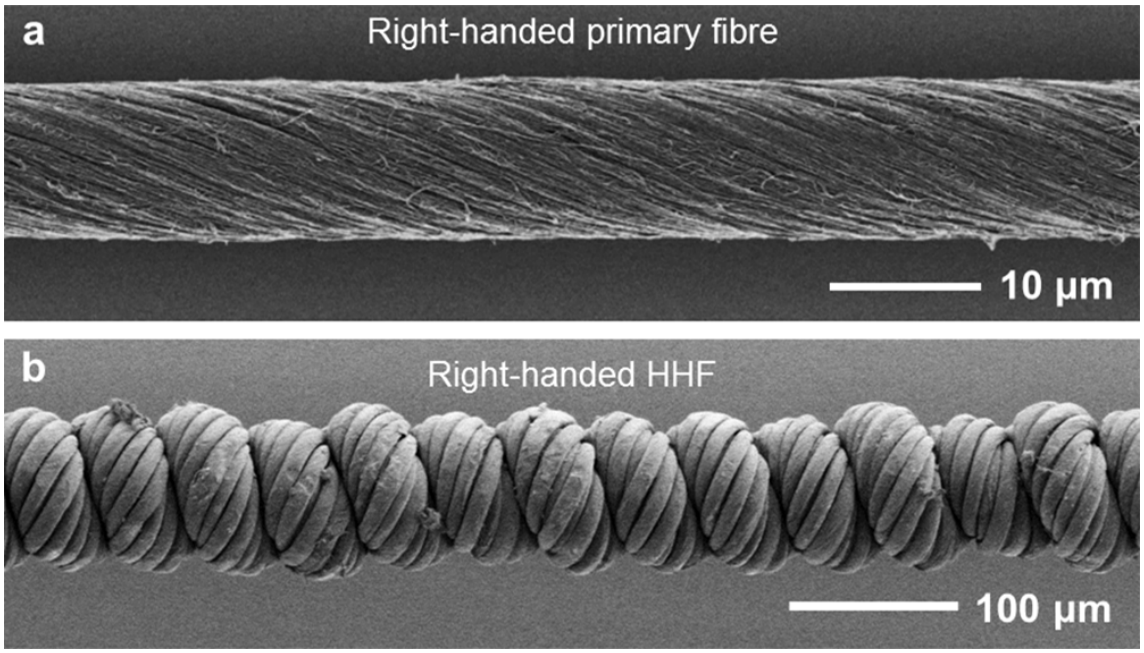

Supplementary Fig. 4. SEM images of a right-handed HHF twisted from 20 right-handed primary fibres. The primary fibres used to construct the HHF share a helical angle of 32 °.

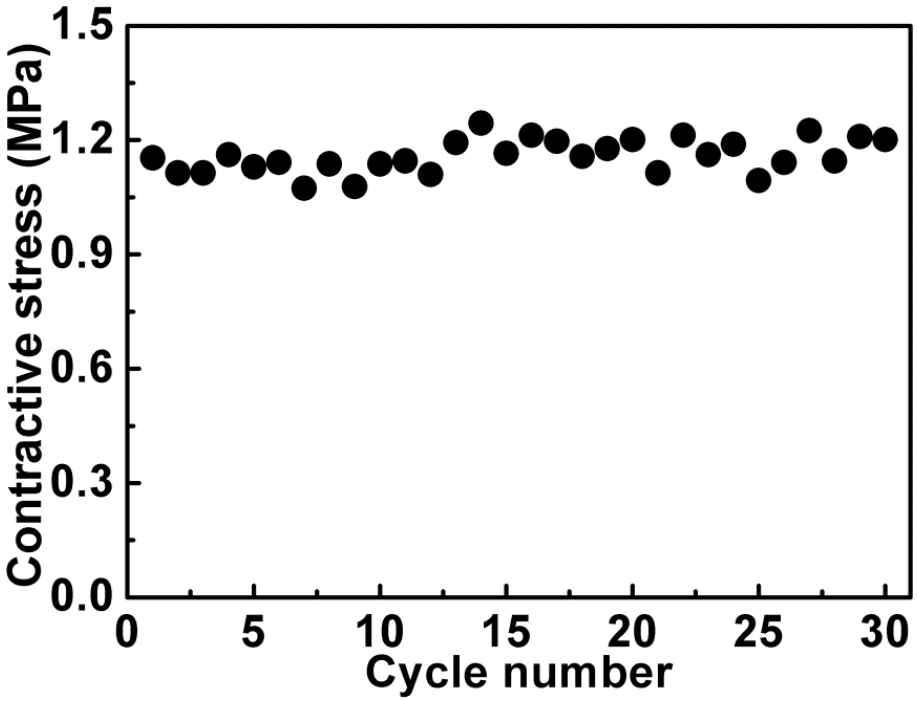

Supplementary Fig. 5. Dependence of the contractive stress generated by an HHF on the cycle number upon coming in contact with a droplet of ethanol. The HHF was twisted from 20 primary fibres.

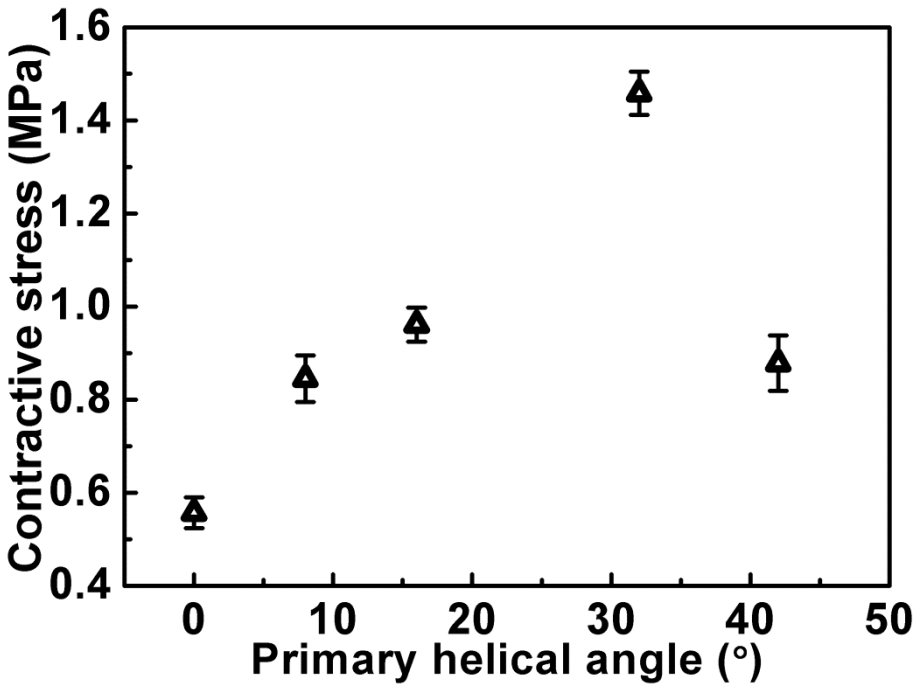

Supplementary Fig. 6. Dependence of the contractive stress generated by an HHF on the helical angle of the primary fibres used to construct the HHF. The HHF was twisted from 20 primary fibres. The error bars are the standard deviation values of five samples.

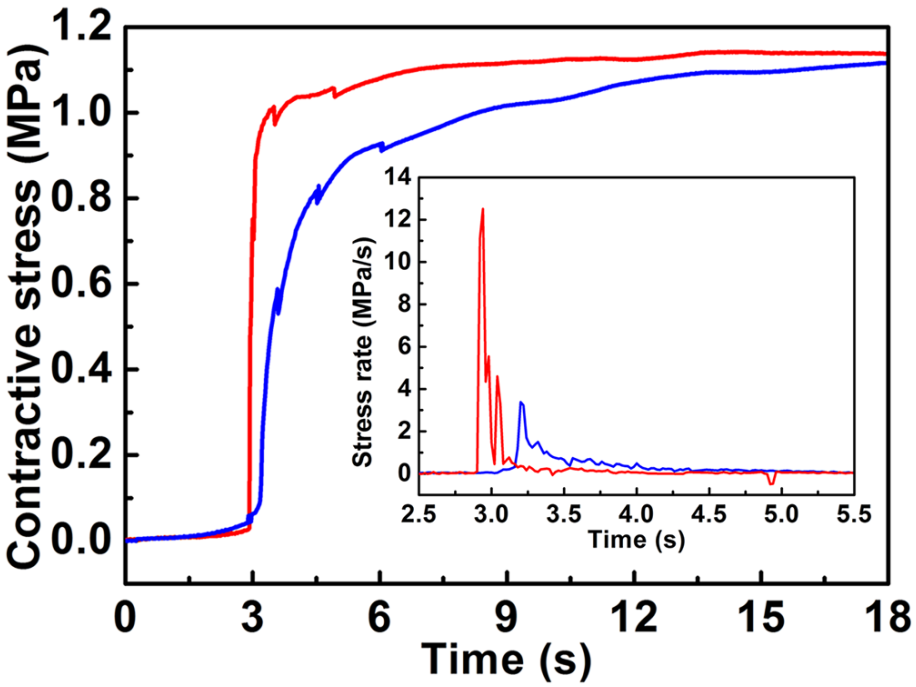

Supplementary Fig. 7. Contraction curve for an HHF (red line) twisted from 40 primary fibres and SHF (blue line) twisted from 40 layers of MWCNT sheets. Corresponding stress rate curves over time are illustrated at the inserted graph. The HHF and SHF generated similar contractive stresses but the former showed a rapider contractive responsiveness.

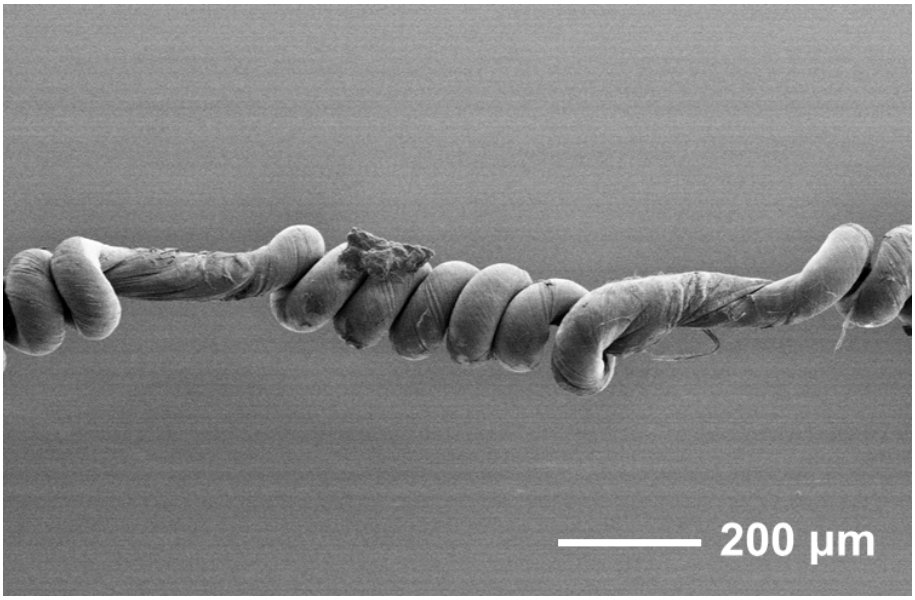

Supplementary Fig. 8. SEM image of an SHF after 15 cycles of actuation. The SHF was twisted from 20 stacked MWCNT sheets.

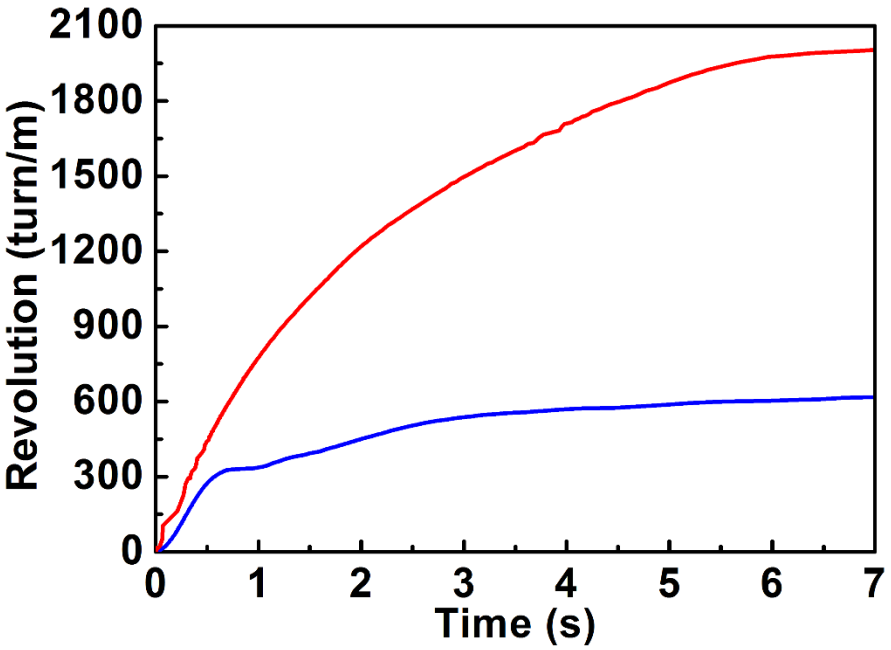

Supplementary Fig. 9. The number of revolutions generated by the HHF (red line) and SHF (blue line) upon absorption of ethanol. Here the HHF was twisted from 20 primary fibres and SHF was twisted from 20 layers of stacked MWCNT sheets.

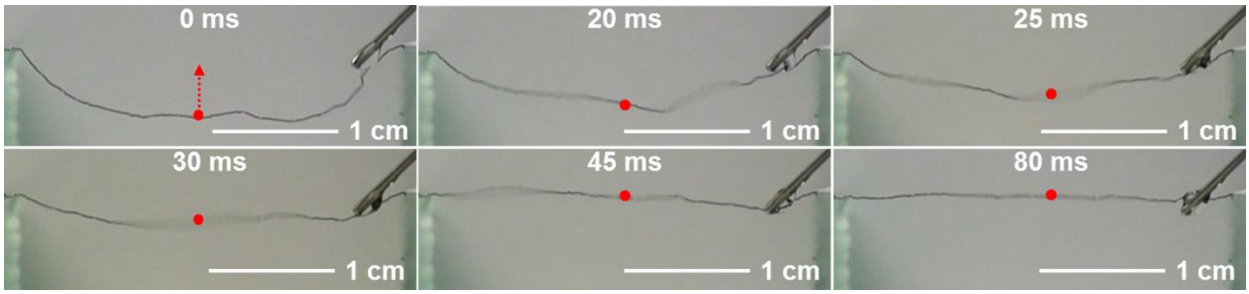

Supplementary Fig. 10. Photographs of the rapid contracting process of a slack HHF. The HHF showed an original length of 3.5 cm. The contracting process can be rapidly completed in 80 ms.

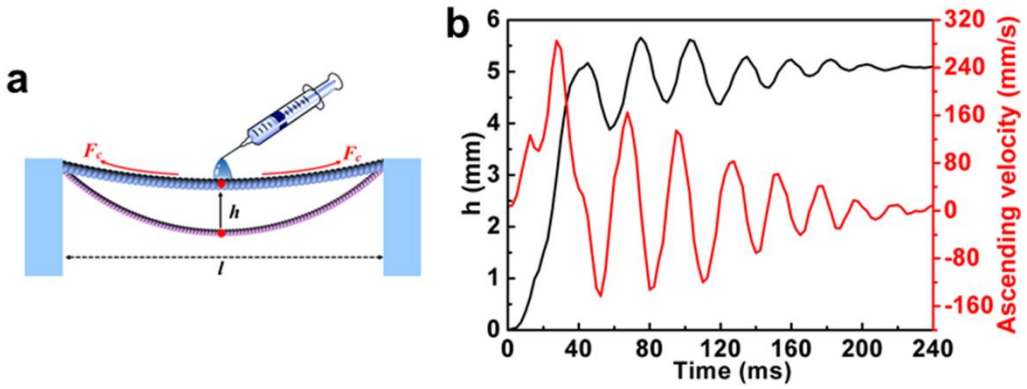

Supplementary Fig. 11. a, Schematic illustration to the experimental setup for the rapid actuation of an slack HHF upon infiltration of ethanol. The ascending distance (*h*) is used to trace the actuation process. **b**, Dependence of the distance ascending (*h*) and the ascending velocity on time upon coming in contact with a droplet of ethanol. The HHF was composed of 20 primary fibres.

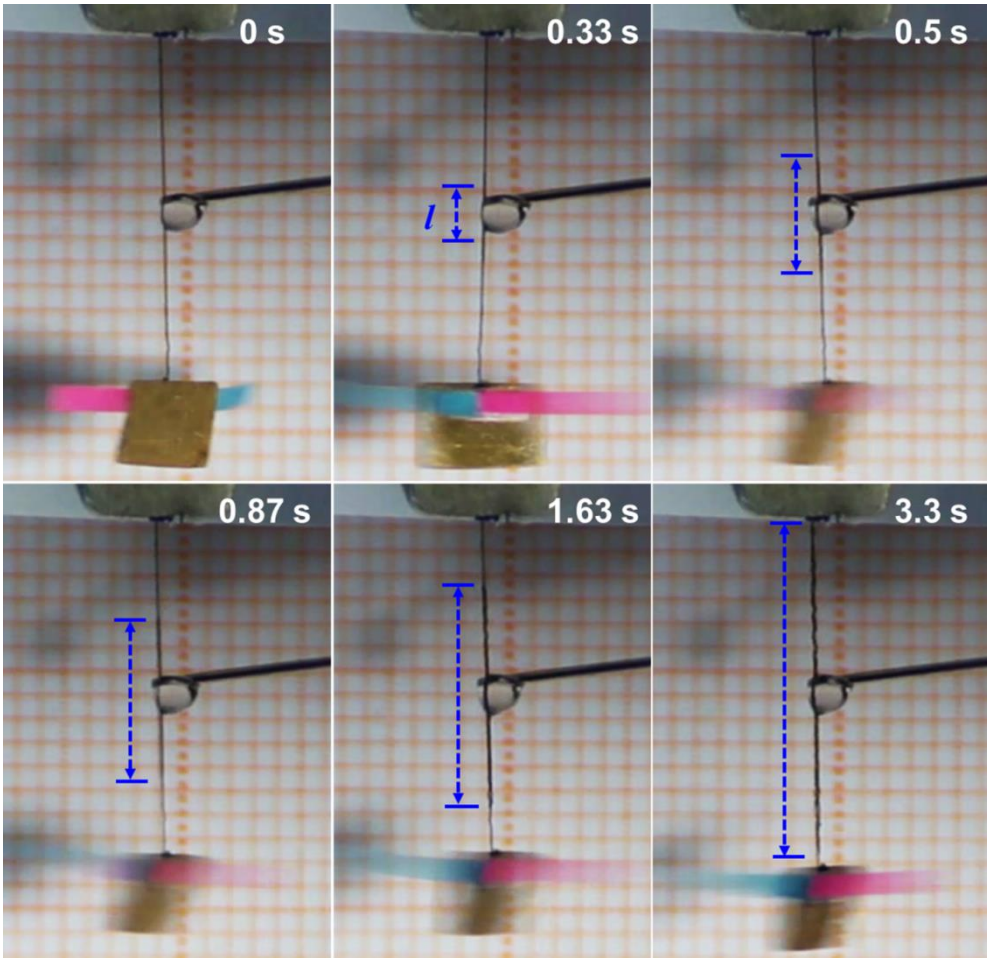

Supplementary Fig. 12. Photographs of an HHF prior to the formation of coiled structure upon coming in contact with an ethanol droplet. The fibre was twisted from 20 primary fibres. The ethanol droplet was gently contacted with the HHF.

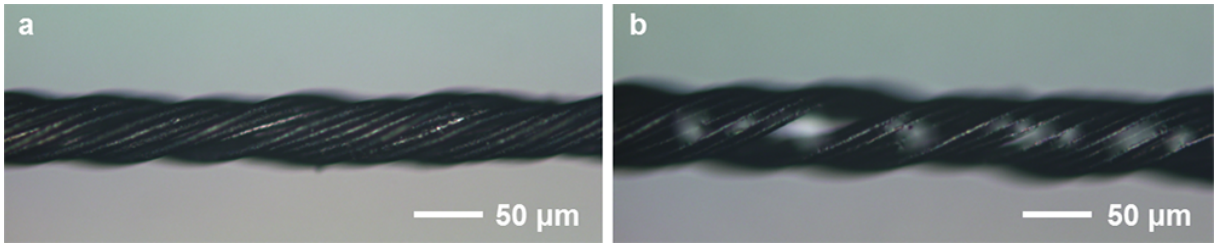

Supplementary Fig. 13. a and **b**, Optical micrographs of a slack HHF without forming a coiled structure before and after infiltration of ethanol, respectively. The HHF was twisted from 20 primary fibres. The two ends of the slack fibre were clamped.

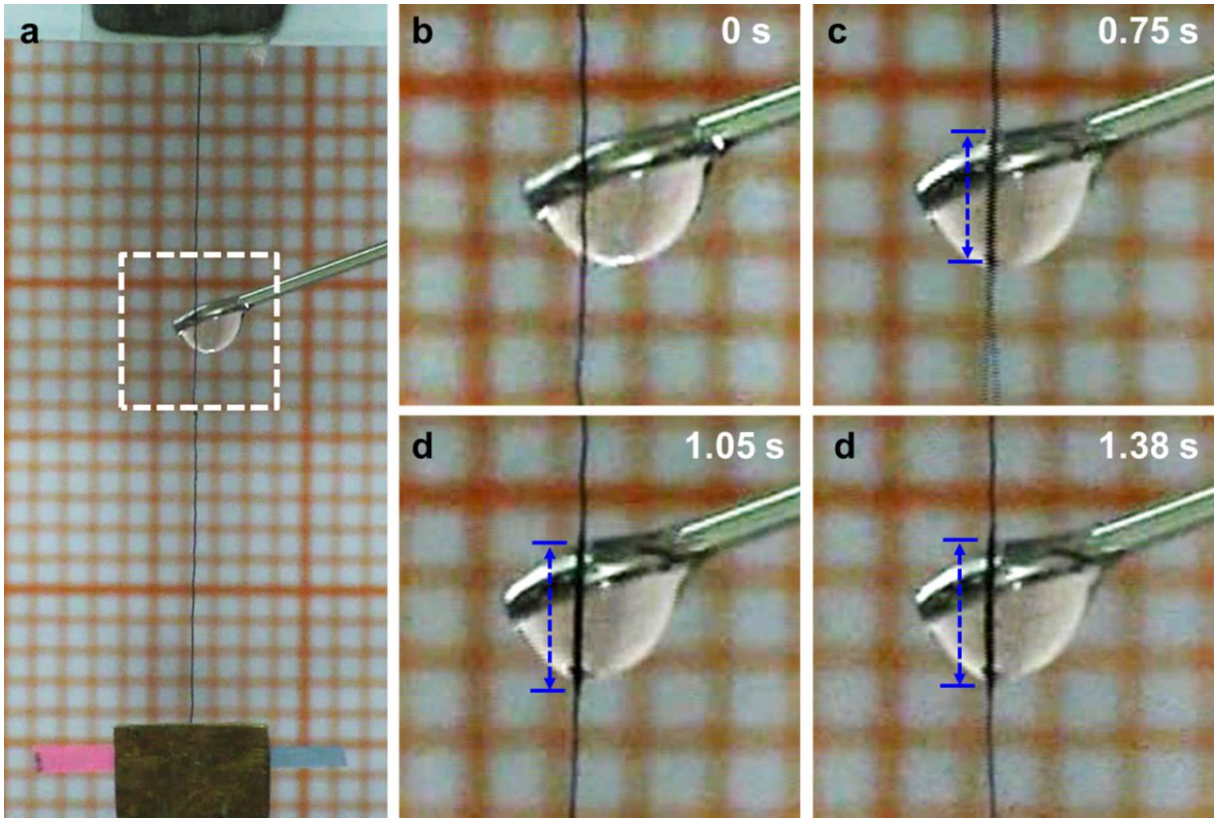

Supplementary Fig. 14. a, Photograph of an SHF prior to the formation of coils upon coming in contact with an ethanol droplet. It was twisted from 20 stacked MWCNT sheets. **b-d**, Enlarged views of the fibre marked with a rectangle at (**a**) after absorption of ethanol. The ethanol droplet was maintained to be gently touched with the SHF during taking the pictures.

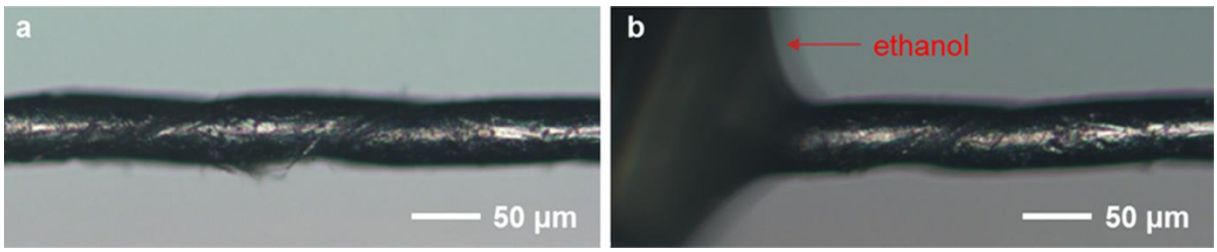

Supplementary Fig. 15. a and **b**, Optical micrographs of a slack SHF without forming a coiled structure before and after infiltration of ethanol, respectively. The SHF was twisted from 20 stacked MWCNT sheets. The two ends of the slack fibre were clamped.

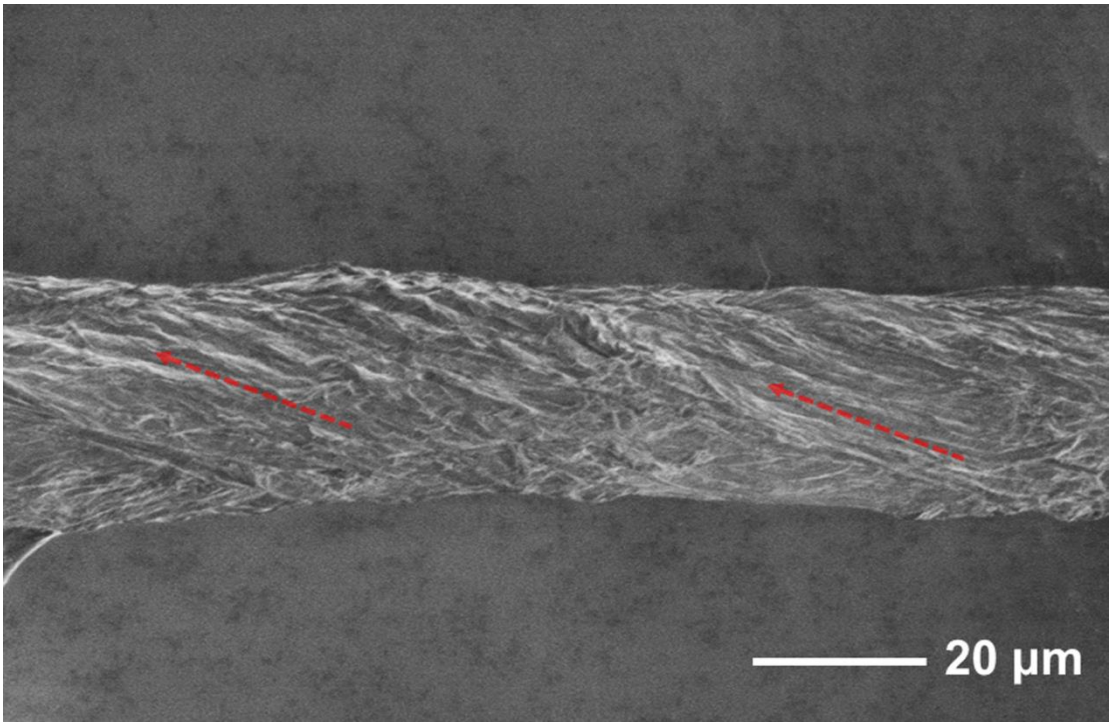

Supplementary Fig. 16. SEM image of a twisted GO fibre. The red arrows indicate that it owns a helical angle of ~30 °.

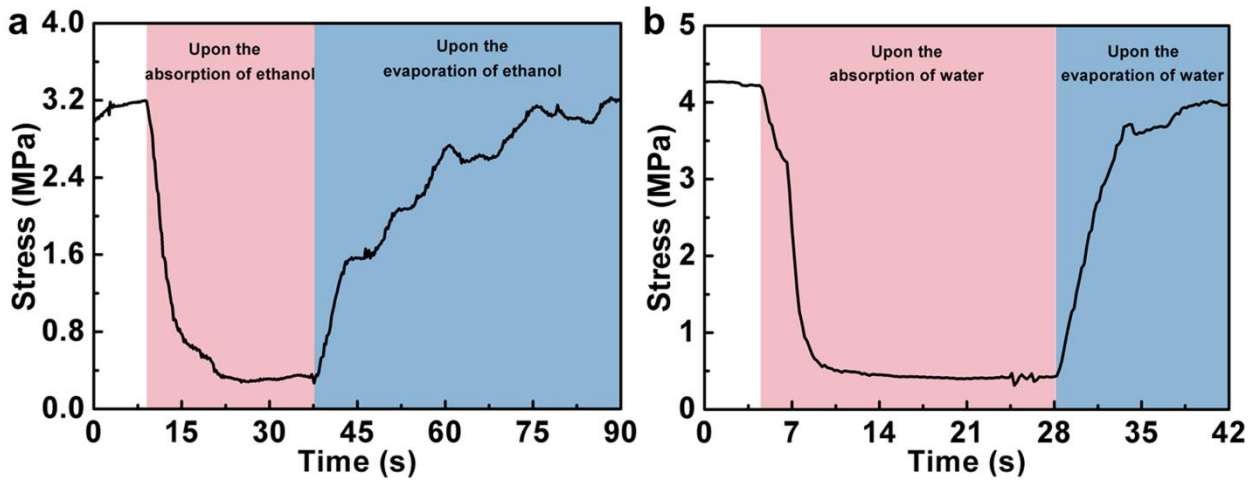

Supplementary Fig. 17. Typical actuation and recovery curves of a twisted GO fibre upon the absorption and subsequent evaporation of ethanol (**a**) and water (**b**). The GO fibre showed slower responses to both ethanol and water.

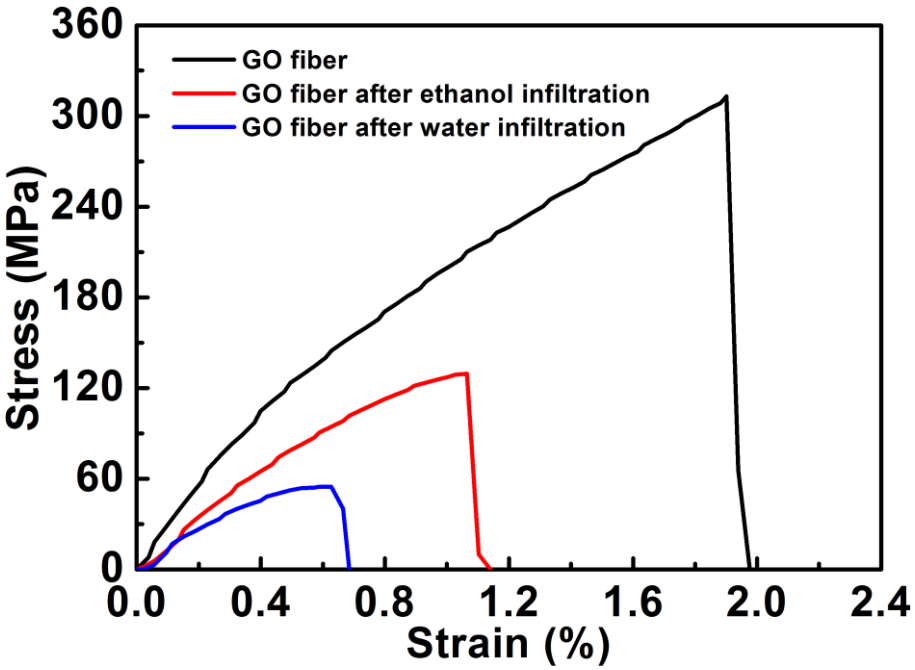

Supplementary Fig. 18. Stress-strain curves of twisted GO fibres before and upon coming into contact with ethanol and water. The tensile strengths were largely decreased after infiltration of solvents.

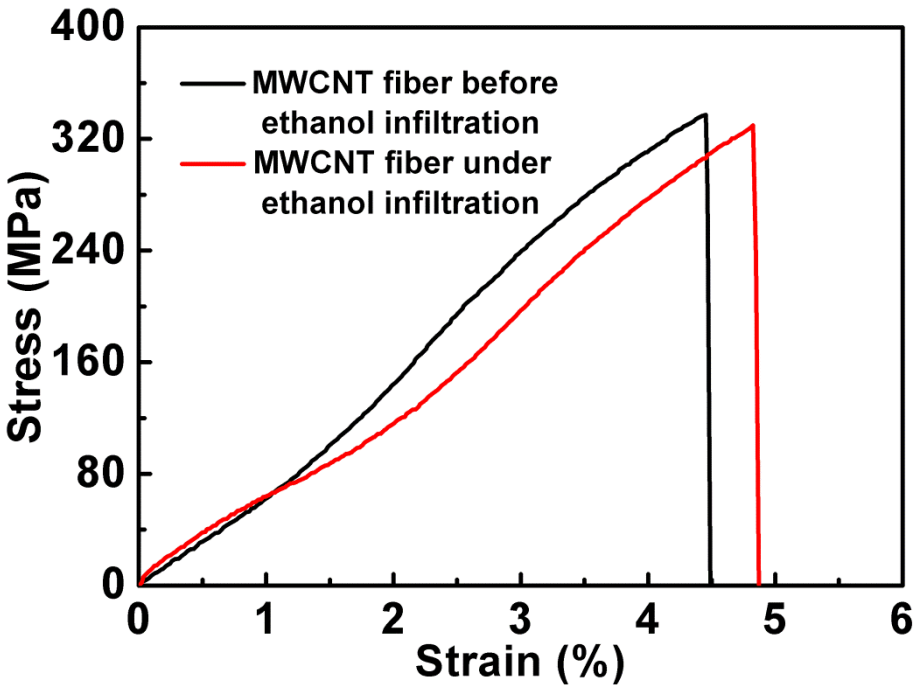

Supplementary Fig. 19. Stress-strain curves of a primary MWCNT fibre before and under ethanol infiltration. The tensile strength can be maintained after the solvent infiltration in the primary fibre.

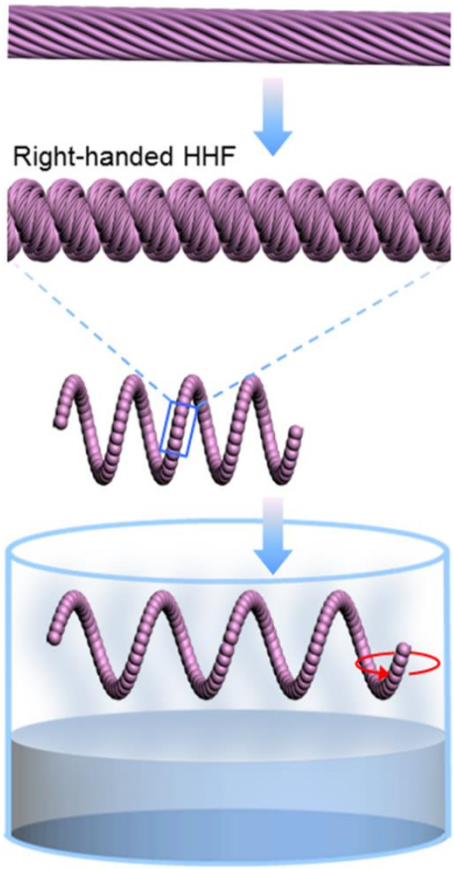

Supplementary Fig. 20. Schematic illustration to the elongation of the spring prepared from a right-handed HHF. The right-handed HHF itself generates a counterclockwise rotation (indicated by the red arrow) to induce the longation when the spring is brought within close proximity to the liquid surface.

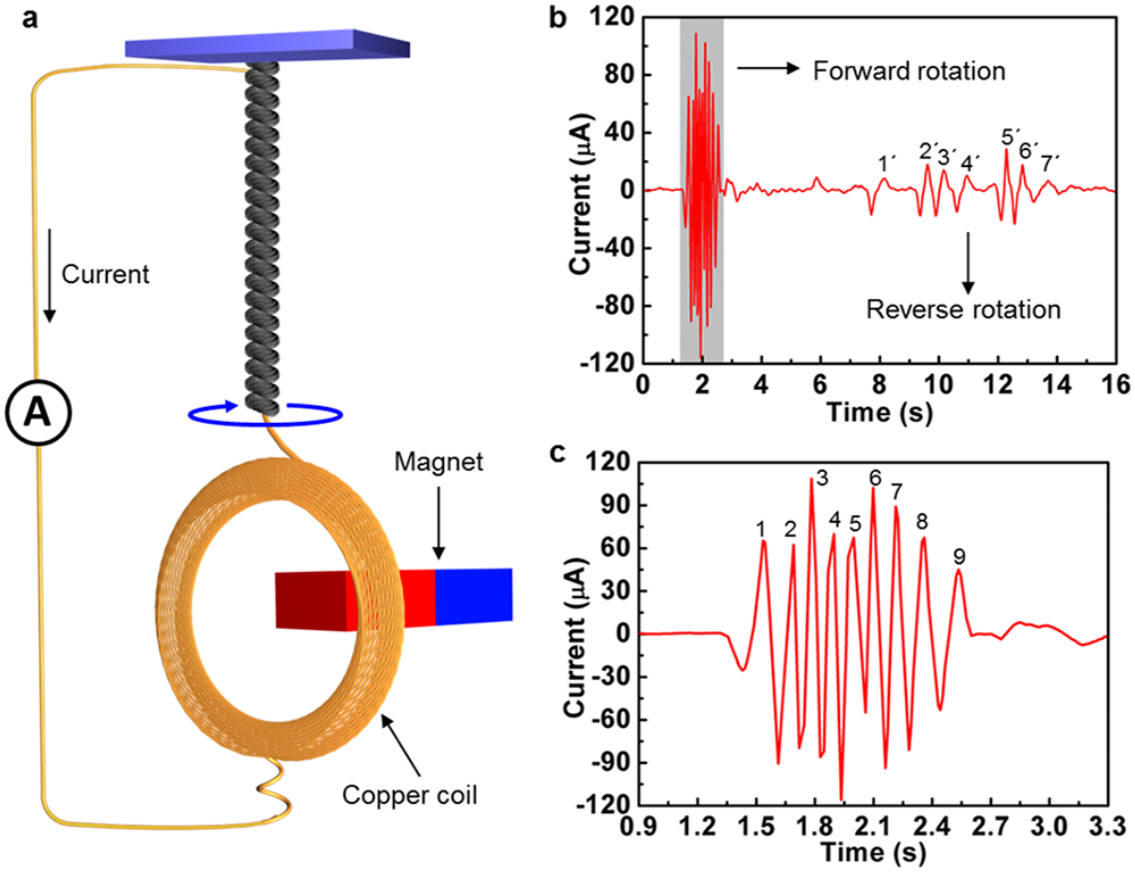

Supplementary Fig. 21. An alternating-current generator based on the solvent-induced rotation of an HHF. **a**, Schematic illustration to the experimental equipment. A homemade copper coil (100 turns) with a diameter of 1.3 cm was connected at one end of an HHF (with a length of 4 cm) twisted from 50 primary fibres. The copper coil was then placed in a magnetic field produced by a bar magnet. Here the HHF also served as a conductive wire. **b**, Alternating currents generated due to the forward and reverse rotations. The HHF was sprayed with ethanol. **c**, Enlarged view of the gray region at **b**. The labelled numbers above the curve represent the rotation numbers.

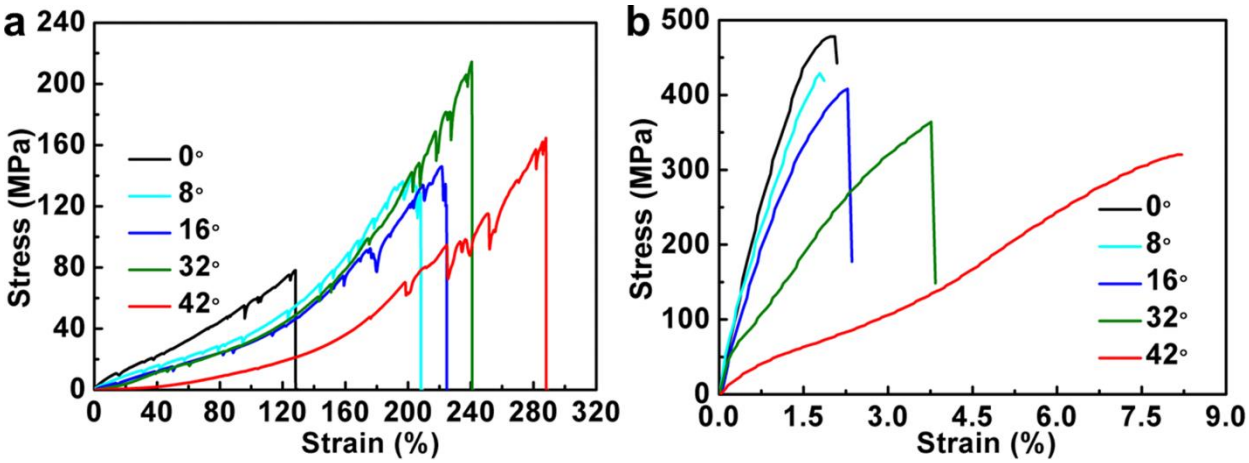

Supplementary Fig. 22. Stress-strain curves of HHFs (**a**) and corresponding left-handed primary fibres (**b**) with helical angles of 0 °, 8 °, 16 °, 32 ° and 42 °, respectively. The strains at breaking in the HHFs were much higher than the building primary fibres.

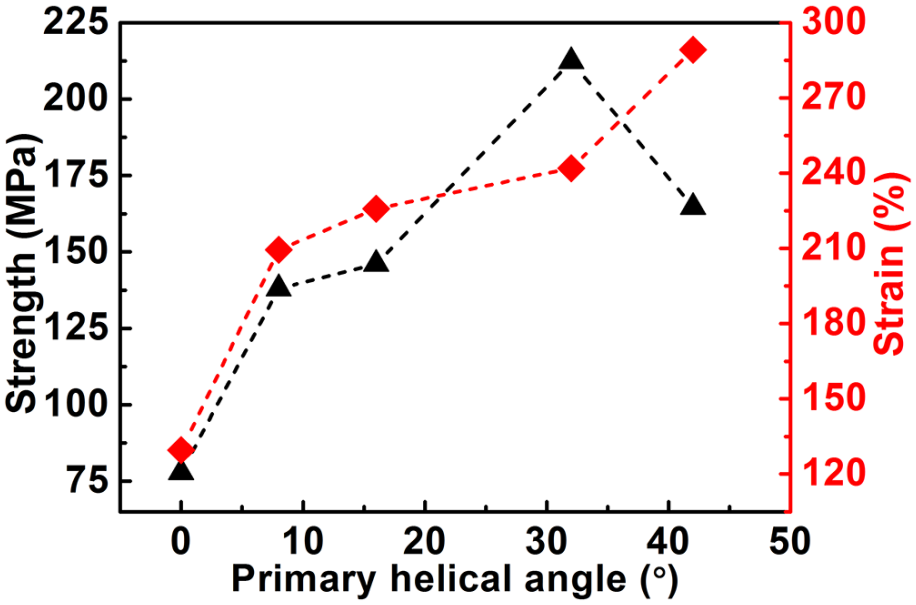

Supplementary Fig. 23. Dependence of strength (black symbol) and strain (red symbol) of HHF on helical angle of building primary fibre. The peak strength occurred at the helical angle of primary fibre to be 32°.

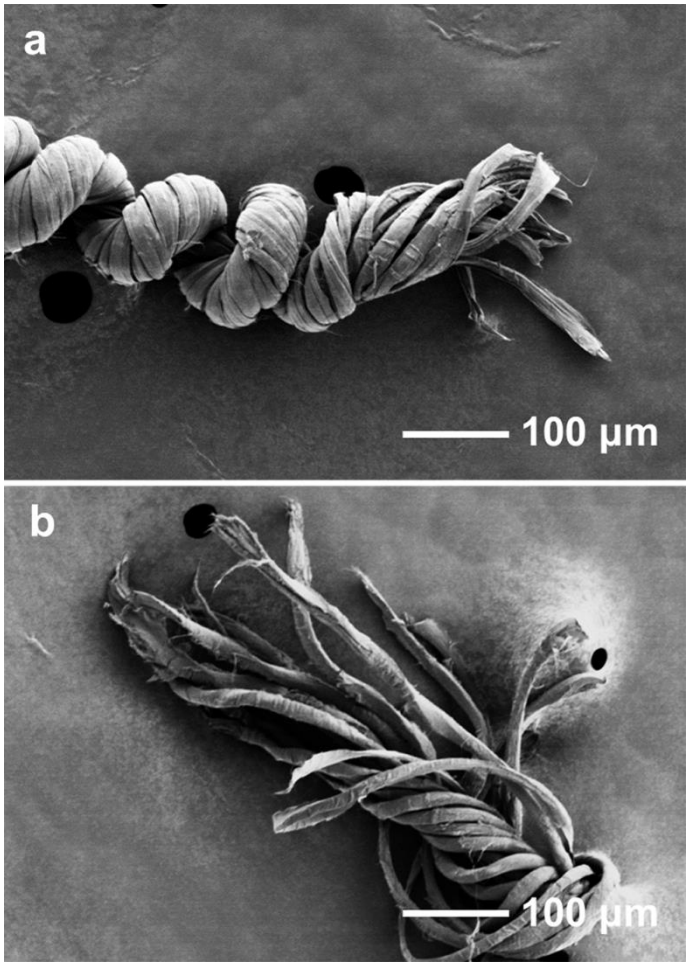

Supplementary Fig. 24. a and **b**, SEM images of HHFs prepared from primary fibres with helical angles of 0 ° and 32 ° after breaking, respectively. They broke under tensile forces during the measurement for stress-strain curves.

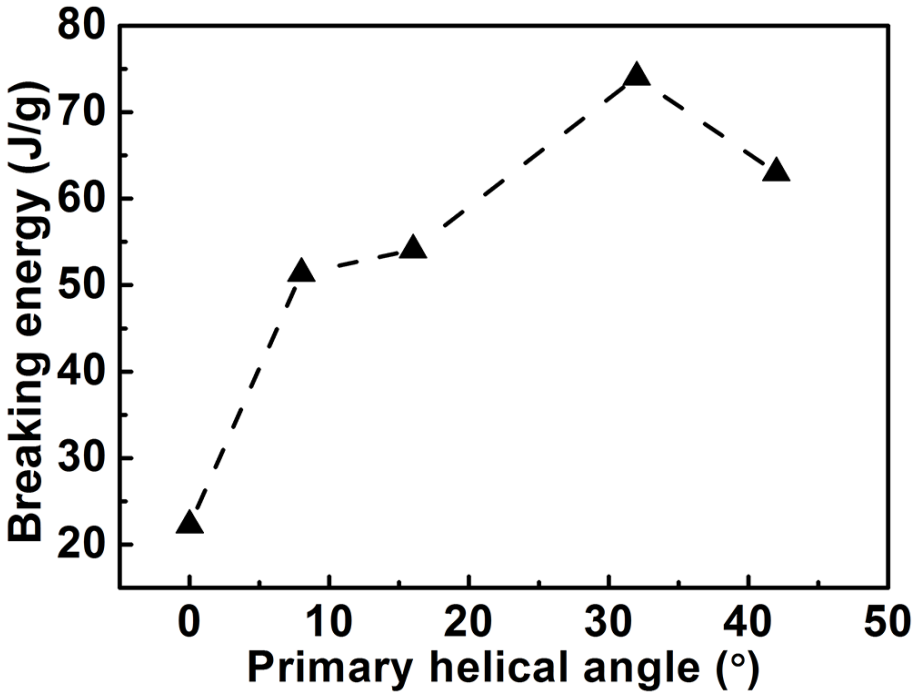

Supplementary Fig. 25. Dependence of breaking energy of HHF on helical angle of building primary fibre. The maximum breaking energy was observed at a helical angle of 32°.

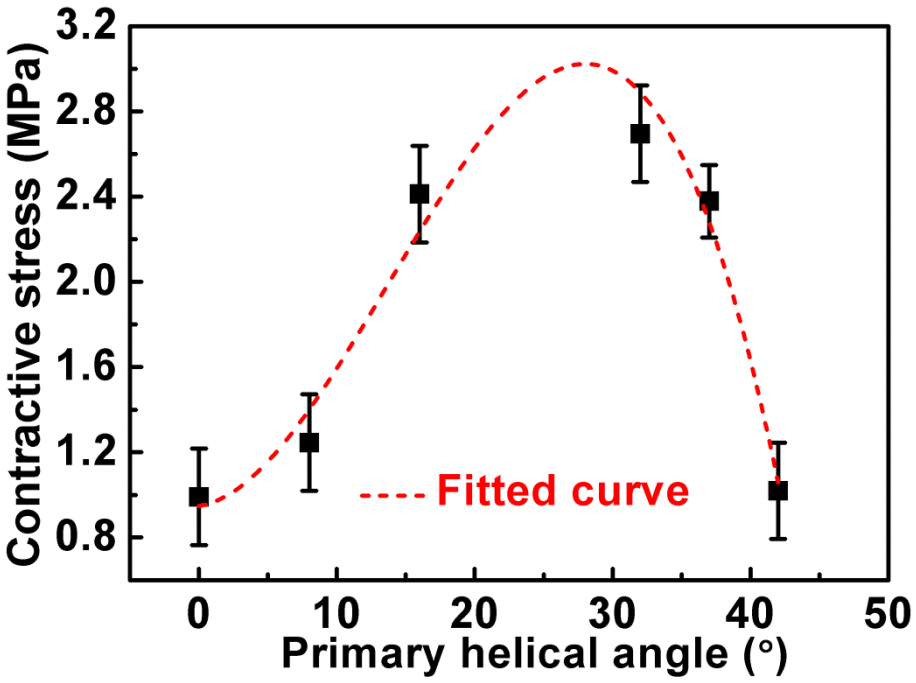

Supplementary Fig. 26. Dependence of contractive stress of primary fibre on the primary helical angle. The error bars are the standard deviation values of five simples.

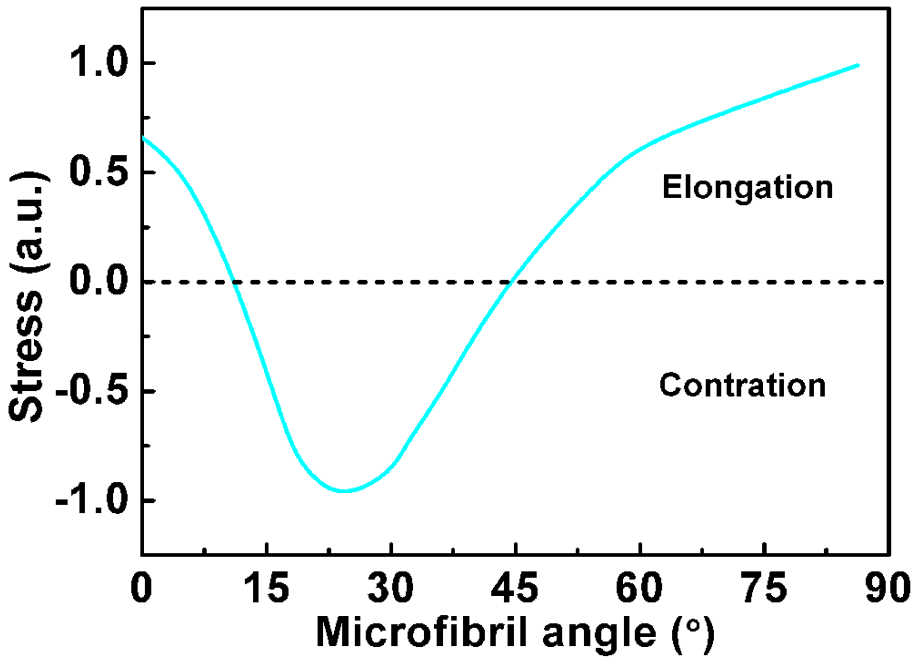

Supplementary Fig. 27. Dependence of generated stress by cylindrical cell on the microfibril angle upon swelling. Here the stress is normalized according to the maximum value. Reproduced with permission from ref. [S1].

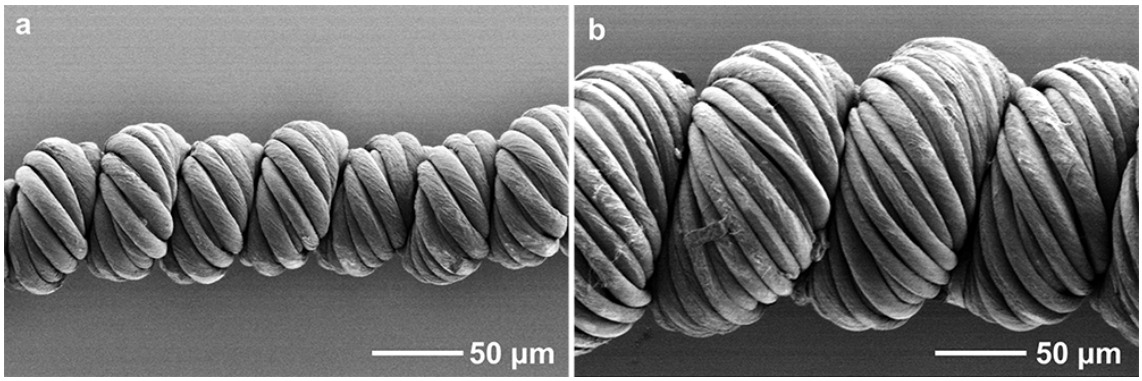

Supplementary Fig. 28. a and **b**, SEM images of HHFs twisted from 10 and 40 primary fibres, respectively. The coils were compactly arranged under both cases.

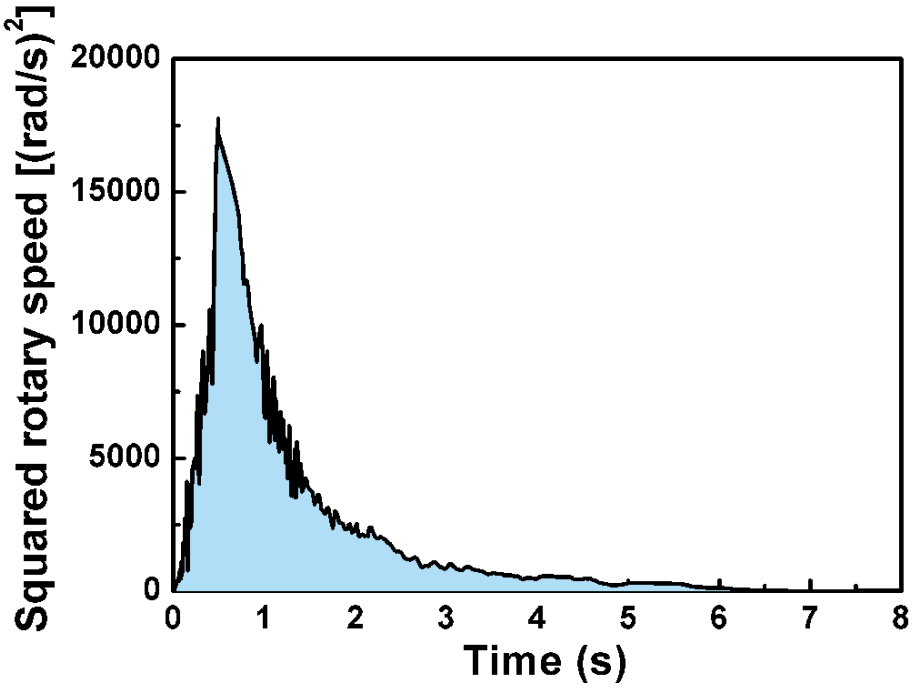

Supplementary Fig. 29. Dependence of the squared rotary speed on time. The length of the HHF was 2 cm. It was used to calculate the rotational work output.

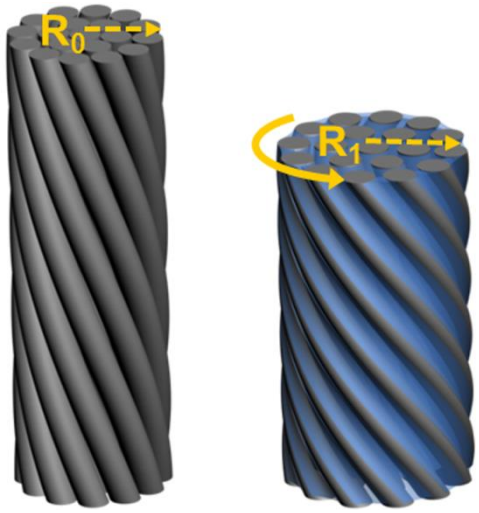

Supplementary Fig. 30. Mechanism of the solvent-induced contraction and rotation of a helix. It expands at the radial direction and contracts along the axial direction after exposure to a solvent.

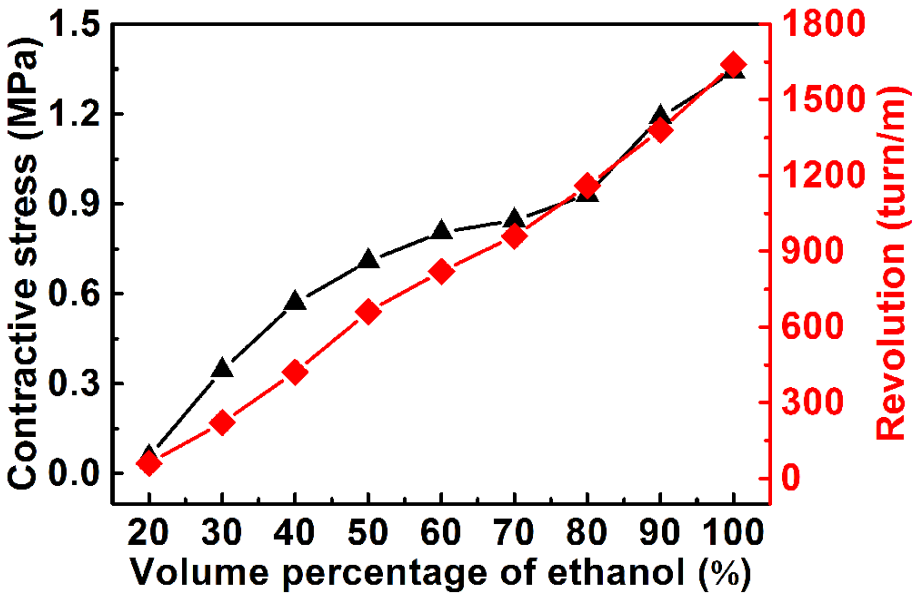

Supplementary Fig. 31. Dependence of the contractive stress and the number of revolutions generated by an HHF on the volume percentage of ethanol. The ethanol/water droplet was used to induce contraction and rotation. Both contractive stress and revolution number were increased with the increasing volume percentage of ethanol.

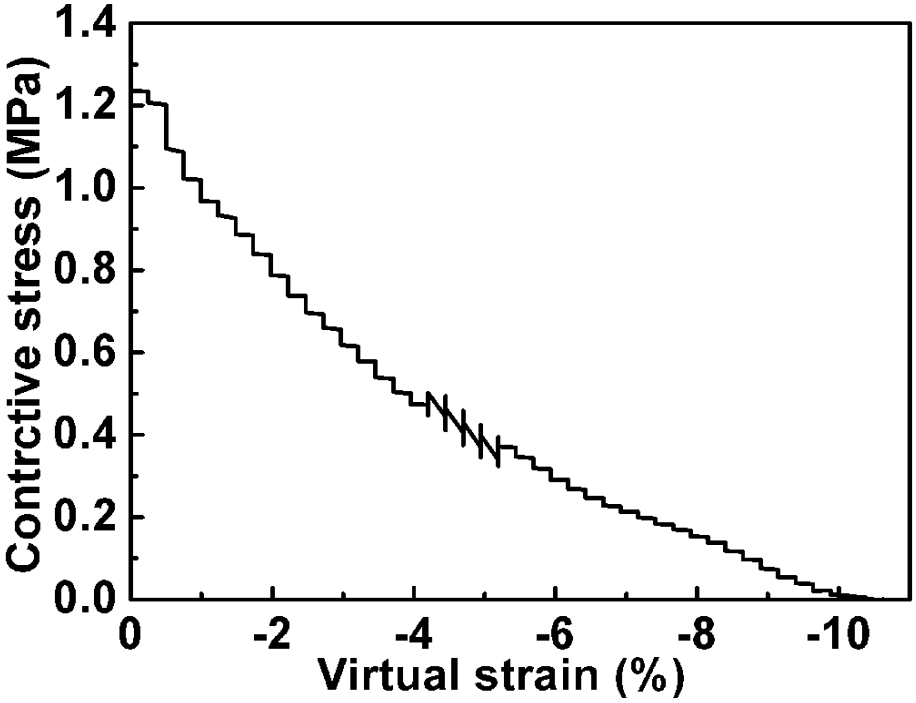

Supplementary Fig. 32. Release curve of stress in an HHF with a helical angle of 32 °. A droplet of ethanol was maintained in touching the HHF during the downward movement (1 mm/min) of the clamp.

Supplementary Table 1. Comparisons between HHF actuator and previous reported actuators[S2, S7-S9].

	This work	**MWCNT yarn muscle**[S2, S7]	**Hybrid MWCNT yarn muscle**[S8]	**Coiled polymer fibre muscle**[S9]
Structure	Hierarchically arranged helical fibre twisted from multiply primary fibres	MWCNT yarn	Hybrid MWCNT yarn filled with wax	Coiled polymer fibre coated with conductive sheet
Stimulus	Solvent and vapour	Electricity	Heating	Heating
Media	Air	Electrolyte	Air	Air
Mechanism	Solvent infiltration driven by capillary force	Electrochemical operation	Volume expansion of wax by heating	Volume expansion of the polymer fibre by heating
Contractive strain (%)	10-15	< 1	10	49
Responding time	45 ms	Hundreds of milliseconds	Hundreds of milliseconds	> 500 ms
Revolution (turn/m)	2,050	694*	48*	14
Rotary speed (rpm per metre)	6,361	590*	12,000*	—

*The two ends of the fibre are clamped in the measurement.

Supplementary Table 2. Comparisons between HHFs twisted from primary MWCNT fibres and SHFs twisted from stacked MWCNT sheets.

	HHF twisted from 20 primary fibres*	**SHF twisted from 20 layers of stacked sheets****
Tensile strength (MPa)	212	91
Breaking strain (%)	240	190
Breaking energy (J/g)	74	44
Contractive stress (MPa)	1.0-1.5	1.0-1.5
Maximum stress rate (MPa/s)	8.4	2.8
Contractive strain (%)	15	9
Responding time (ms)	~44	>300
Maximum strain rate (%/s)	340	30
Revolution (turn/m)	2,050	620
Maximum rotary speed (rpm per metre)	6,361	760

*The primary fibres show the same helical angle of 32°. The average number of coils per millimetre is 20, the average diameter of the HHF is 105 μm and the average diameter of the coil is 55 μm.

**The average number of coils per millimetre is 16, the average diameter of the SHF is 115 μm and the average diameter of the coil is 60 μm.

Captions for Supplementary Movies

Supplementary Movie 1. Contraction and clockwise rotation of a left-handed HHF (length of ~2 cm) that is assembled from 20 primary fibres upon coming in contact with an ethanol droplet. It uplifts a copper paddle that is 570 times heavier than the fibre.

Supplementary Movie 2. Contraction and counterclockwise rotation of a right-handed HHF (length of ~2 cm) that is assembled from 20 right-handed fibres upon coming in contact with an ethanol droplet. The copper paddle is the same to the Supplementary Movie 1.

Supplementary Movie 3. Slow-motion video of a contractive actuation generated by a slack HHF upon coming in contact with an ethanol droplet. The HHF is stabilized at the two ends.

Supplementary Movie 4. Contraction and relaxation of an HHF (with a load) upon absorption and evaporation of ethanol.

Supplementary Movie 5. Fluorescent slow-motion video of the infiltration process for the twisted primary fibres prior to the formation of the coiled structure upon absorption of a rhodamine/ethanol solution (concentration of 0.1 mg/mL).

Supplementary Movie 6. Contractive and rotary actuation of an HHF (the same to Supplementary Movie 1) in response to a dichloromethane vapour.

Supplementary Movie 7. Contractive deformation of a spring being prepared from an HHF that is assembled from 20 primary fibres in response to the dichloromethane vapour.

Supplementary Movie 8. Elongation deformation of a spring being prepared from an right-handed HHF that is assembled from 20 right-handed primary fibres in response to the dichloromethane vapour.

Supplementary Movie 9. A smart textile woven from HHFs uplifts a copper ball that is 100 times heavier than the textile for 4.5 mm within milliseconds upon spraying of ethanol.

Supplementary References

[S1] Fratzl, P. & Barth, F. G. Biomaterial systems for mechanosensing and actuation. *Nature* **462**, 442-448 (2009).

[S2] Foroughi, J. *et al.* Torsional carbon nanotube artificial muscles. *Science* **334**, 494-497 (2011).

[S3] Trivedi, D., Rahn, C. D., Kier, W. M. & Walker, I. D. Soft robotics: Biological inspiration, state of the art, and future research. *Appl. Bionics Biomech.* **5**, 99-117 (2008).

[S4] Qiu, J. *et al.* Liquid Infiltration into Carbon Nanotube Fibres: Effect on Structure and Electrical Properties. *ACS Nano* **7**, 8412-8422 (2013).

[S5] Peigney, A., Laurent, C., Flahaut, E., Bacsa, R. & Rousset, A. Specific surface area of carbon nanotubes and bundles of carbon nanotubes. *Carbon* **39**, 507-514 (2001).

[S6] Bertinetti, L., Fischer, F. & Fratzl, P. Physicochemical Basis for Water-Actuated Movement and Stress Generation in Nonliving Plant Tissues. *Phys. Rev. Lett.* **111** (2013).

[S7] Mirfakhrai, T. *et al.* Electrochemical actuation of carbon nanotube yarns. *Smart Mater. Struct.* **16**, S243-S249 (2007).

[S8] Lima, M. D. *et al.* Electrically, chemically, and photonically powered torsional and tensile actuation of hybrid carbon nanotube yarn muscles. *Science* **338**, 928-932 (2012).

[S9] Haines, C. S. *et al.* Artificial muscles from fishing line and sewing thread. *Science* **343**, 868-872 (2014).